01 Aug 2022

Elevated Temperature Thermal Properties of ZrB2-B4C Ceramics

Eric W. Neuman

Matthew Thompson

William Fahrenholtz
Missouri University of Science and Technology, billf@mst.edu

Gregory E. Hilmas
Missouri University of Science and Technology, ghilmas@mst.edu

Recommended Citation

Short communication

Elevated temperature thermal properties of ZrB$_2$-B$_4$C ceramics

Eric W. Neuman [1], Matthew Thompson [2], William G. Fahrenholtz [*], Gregory E. Hilmas

Missouri University of Science and Technology, Rolla, MO 65409, United States

ARTICLE INFO

ABSTRACT

The elevated temperature thermal properties of zirconium diboride ceramics containing boron carbide additions of up to 15 vol% were investigated using a combined experimental and modeling approach. The addition of B$_4$C led to a decrease in the ZrB$_2$ grain size from 22 μm for nominally pure ZrB$_2$ to 5.4 μm for ZrB$_2$ containing 15 vol% B$_4$C. The measured room temperature thermal conductivity decreased from 93 W/m·K for nominally pure ZrB$_2$ to 80 W/m·K for ZrB$_2$ containing 15 vol% B$_4$C. The thermal conductivity also decreased as temperature increased. For nominally pure ZrB$_2$, the thermal conductivity was 67 W/m·K at 2000 °C compared to 55 W/m·K for ZrB$_2$ containing 15 vol% B$_4$C. A model was developed to describe the effects of grain size and the second phase additions on thermal conductivity from room temperature to 2000 °C. Differences between model predictions and measured values were less than 2 W/m·K at 25 °C for nominally pure ZrB$_2$ and less than 6 W/m·K when 15 vol% B$_4$C was added.

1. Introduction

Zirconium diboride (ZrB$_2$) is in a class of materials known as ultra-high temperature ceramics (UHTCs). ZrB$_2$ is in this class because it has a melting temperature above 3000 °C along with high thermal and electrical conductivities [1–5]. This unusual combination of properties makes ZrB$_2$ an excellent candidate for applications in extreme environments such as high temperature electrodes, thermal protection systems, and molten metal crucibles [6]. The high thermal and electrical conductivities arise from the significant electron contribution, which can be > 70% at room temperature [5]. For example, the total thermal conductivity can be above 90 W/m·K at room temperature with > 60 W/m·K from the electron contribution [5,7].

ZrB$_2$ and other transition metal borides and carbides have strong covalent bonding and low self-diffusion coefficients. As a result, a combination of temperatures of 1900 °C or higher with applied external pressure is normally required to achieve full density [8–11]. Oxygen impurities in the form of ZrO$_2$ and B$_2$O$_3$ on particle surfaces have been shown to cause grain coarsening preferentially to densification at elevated temperatures [12]. Additives such as carbon, B$_4$C, and WC that react with and remove oxide impurities are used to promote densification [12,13]. Excess additives can form isolated particles, solid solutions, and/or grain boundary phases in the densified ceramics, which

impact mechanical, electrical, and thermal properties [13,14]. Specifically for thermal properties, reported room temperature thermal conductivity values for polycrystalline ZrB$_2$ based ceramics vary widely, from as low as 29 W/m·K to as high as ~140 W/m·K [14–17]. Hence, changes to processing conditions and composition can significantly impact thermal properties. Several types of models have been used to describe the thermal conductivity of diboride based ceramics including network conductance models [18], grain size models [14], and effective medium theories, but these are typically limited to evaluating one specific composition [19].

The purpose of this study was to measure and model the thermal conductivity of ZrB$_2$ ceramics as a function of B$_4$C content. More generally, the study evaluated the impact of isolated, electrically insulating particles on the thermal conductivity of a conductive matrix.

2. Materials and methods

2.1. Processing

Commercially available ZrB$_2$ (Grade B, H.C. Starck, Goslar, Germany) with a reported purity of 98.2%, an average particle size of 2 μm, and a reported Hf impurity of 1.9 wt% and B$_4$C (Grade HS, H.C. Starck) with a reported purity of > 96.8%, a B/C ratio of 3.8, and starting

---

particle sizes that ranged from 0.6 to 1.2 μm, were used for this study. The ZrB_2 powder was batched with 0, 1, 2, 5, 10, and 15 vol% B_4C and ball milled in hexanes for one hour using ZrB_2 milling media. The B_4C sample was prepared using the same processes as the ZrB_2-B_4C ceramics. The resulting slurry was dried by rotary evaporation. The mass of the ZrB_2 milling media was measured before and after milling, showing that ~0.1 wt% additional ZrB_2 was incorporated into the powders. After rotary evaporation, the powders were passed through a 50-mesh sieve.

Densification was accomplished by hot-pressing using a 1-inch diameter graphite die in a resistively heated graphite element hot-press (Model HP20–3060–20, Thermal Technology Inc., Santa Rosa, CA). The graphite die was lined with graphite paper and coated with boron nitride (SP-108, Cerac, Milwaukee, WI) to minimize reaction between the die and the powders. Specimens were heated at 40 °C/min throughout the run. Below 1500 °C, specimens were heated in a mild vacuum (~20 Pa). Isothermal holds of 1 h were used at 1300 °C and 1500 °C during heating to allow for evaporation of B_2O_3 and/or reaction of ZrO_2 and B_2O_3 with B_4C. After the hold at 1500 °C, the atmosphere was changed to flowing Ar at a pressure of ~10^5 Pa and a uniaxial pressure of 32 MPa was applied. The furnace was held at 2100 °C until ram travel had stopped for 10 min. The furnace was then allowed to cool at 40 °C/min. The applied pressure was released when the furnace reached 1500 °C.

Hot-pressed specimens were surface ground and cut (FSG-3A818, Chevalier, Santa Fe Springs, CA) into squares prisms approximately 12.5 mm × 12.5 mm× 3 mm. The outer portions of the billets were ground or cut away to remove the portion of the pellet that may have been affected by reaction with the hot-press die.

2.2. Characterization

The bulk density of each specimen was measured by the Archimedes' method (ASTM standard C373) using vacuum infiltration with distilled water as the immersing medium. Specimens were polished using successively finer diamond abrasives with a final size of 0.25 μm. Scanning electron microscopy (SEM; Hitachi S570, Japan) was used to characterize microstructure. Grain sizes were measured from SEM micrographs using image analysis software (ImageJ, National Institutes of Health, Bethesda, MD) by analyzing ~500 grains.

Thermal diffusivity was measured by the laser flash technique (Flashline 5000, Anter Corp, Pittsburgh, PA) according to ASTM E1461. Specimens were coated with graphite (Dry Graphite Lube, Diversified Brands, Cleveland, OH), then measured by heating at 15 °C/min to the test temperature, 2000 °C maximum test temperature, in flowing Ar (~41 kPa). Each data point was an average of 3 tests taken at 2 min intervals after the specimen had been held at a constant temperature for 7 min. Results were calculated using the Clark and Taylor method for determining thermal diffusivity, Eq. (1): [20].

$$\alpha = \frac{L^2}{t_{0.5}} \left[-0.346 + 0.362 \left(\frac{t_{0.75}}{t_{0.25}} \right) - 0.065 \left(\frac{t_{0.75}}{t_{0.25}} \right)^2 \right] \qquad (1)$$

Where α is thermal diffusivity, L is specimen thickness, and $t_{0.25}$, $t_{0.5}$, and $t_{0.75}$ are the time for the specimen to rise to a quarter, half, and three quarters of the maximum temperature, respectively, following the laser pulse.

Heat capacity was measured at the same time as thermal diffusivity by comparing the relative temperature rise of each specimen against a graphite standard (Eq. 2),

$$(\rho C_p)_M = \frac{L_R \Delta T_R}{L_M \Delta T_M} (\rho C_p)_R \qquad (2)$$

where ρ is bulk density, C_p is heat capacity, L is specimen thickness, and ΔT is temperature rise of the specimen (M) and graphite standard (R) [21]. The bulk density was calculated as a function of temperature using

Table 1

Summary of density and grain size for the ZrB_2-B_4C ceramics hot-pressed at 2100 °C at 32 MPa in flowing Ar atmosphere.

Sample ID	B_4C Content (vol%)	Bulk Density (g/cm^3)	Theoretical Density (g/cm^3)	Relative Density (%)	Matrix Grain Size (μm)
Z0B	0	5.93	6.10	97.2	22.4 ± 12.0
Z1B	1	6.02	6.07	99.2	14.5 ± 8.8
Z2B	2	5.98	6.03	99.2	15.9 ± 8.2
Z5B	5	5.93	5.94	99.8	12.0 ± 7.1
Z10B	10	5.78	5.80	99.7	9.1 ± 5.1
Z15B	15	5.60	5.62	99.6	5.4 ± 3.1
B_4C	100	2.49	2.52	98.8	3.8 ± 1.0

thermal expansion data for ZrB_2 and B_4C provided by Touloukian [22]. Thermal conductivity (λ) was then calculated at each temperature from the measured thermal diffusivity (α), calculated heat capacity (Cp), and temperature-dependent bulk density (ρ), according to Eq. (3).

$$\lambda = \alpha \rho C_p \qquad (3)$$

2.3. Model development

A model was developed to describe the thermal conductivity behavior of the ZrB_2-B_4C ceramics as a function of B_4C addition and temperature. The approach was to calculate the electron and phonon contributions individually and then sum them to obtain the total thermal conductivity (Eq. 4). The electrical resistivity of B_4C (~10^2 – 10^4 Ω·m, 300–1500 K) [23] is significantly higher than ZrB_2 (~50–800 mΩ·m, 20–2000 °C) [24]. Thus, the electron contribution from B_4C was assumed negligible. The electron contributions were calculated using an effective medium approach (Eq. 5), where λ_{e,ZrB_2} is the electron contribution from ZrB_2 and ν_{B_4C} is the nominal volume fraction of B_4C from batching [19,25]. The electron contribution (λ_e) to the thermal conductivity was calculated from measured electrical resistivity values using the Weidemann-Franz law (Eq. 6) [26], where L is the Lorentz number (2.45 ×10^{-8} W·Ω·K^{-2} reported for ZrB_2) [14], T is the absolute temperature, and ρ is electrical resistivity from a previous study [27]. The phonon contribution was calculated using the Maxwell-Eucken method (Eq. 7) [28] using the measured conductivity of B_4C (λ_{ph,B_4C}) and the phonon contribution data for ZrB_2 (λ_{ph,ZrB_2}) that was calculated in a previous study [27]. In addition, the effect of grain size on the phonon contribution of ZrB_2 was estimated using Eq. (8), where T is the absolute temperature and d is average grain size [29].

$$\lambda = \lambda_e + \lambda_{ph} \qquad (4)$$

$$\lambda_e = \lambda_{e,ZrB_2} \frac{2 - 2\nu_{B_4C}}{2 + \nu_{B_4C}} \qquad (5)$$

$$\lambda_{e,ZrB_2} = \frac{LT}{\rho} \qquad (6)$$

$$\lambda_{ph} = \lambda_{ph,ZrB_2} \left(\frac{(2\lambda_{ph,ZrB_2} + \lambda_{ph,B_4C}) - 2(\lambda_{ph,ZrB_2} - \lambda_{ph,B_4C})\nu_{B_4C}}{(2\lambda_{ph,ZrB_2} + \lambda_{ph,B_4C}) - (\lambda_{ph,ZrB_2} - \lambda_{ph,B_4C})\nu_{B_4C}} \right) \qquad (7)$$

$$\lambda_{ph,ZrB_2} = \left(1.7x10^{-4}T + \frac{8.7x10^{-8}}{d} \right)^{-1} \qquad (8)$$

3. Results and discussion

Table 1 summarizes the specimen designations and bulk density information. For nominally pure ZrB_2, the bulk density was 5.93 g/cm^3,
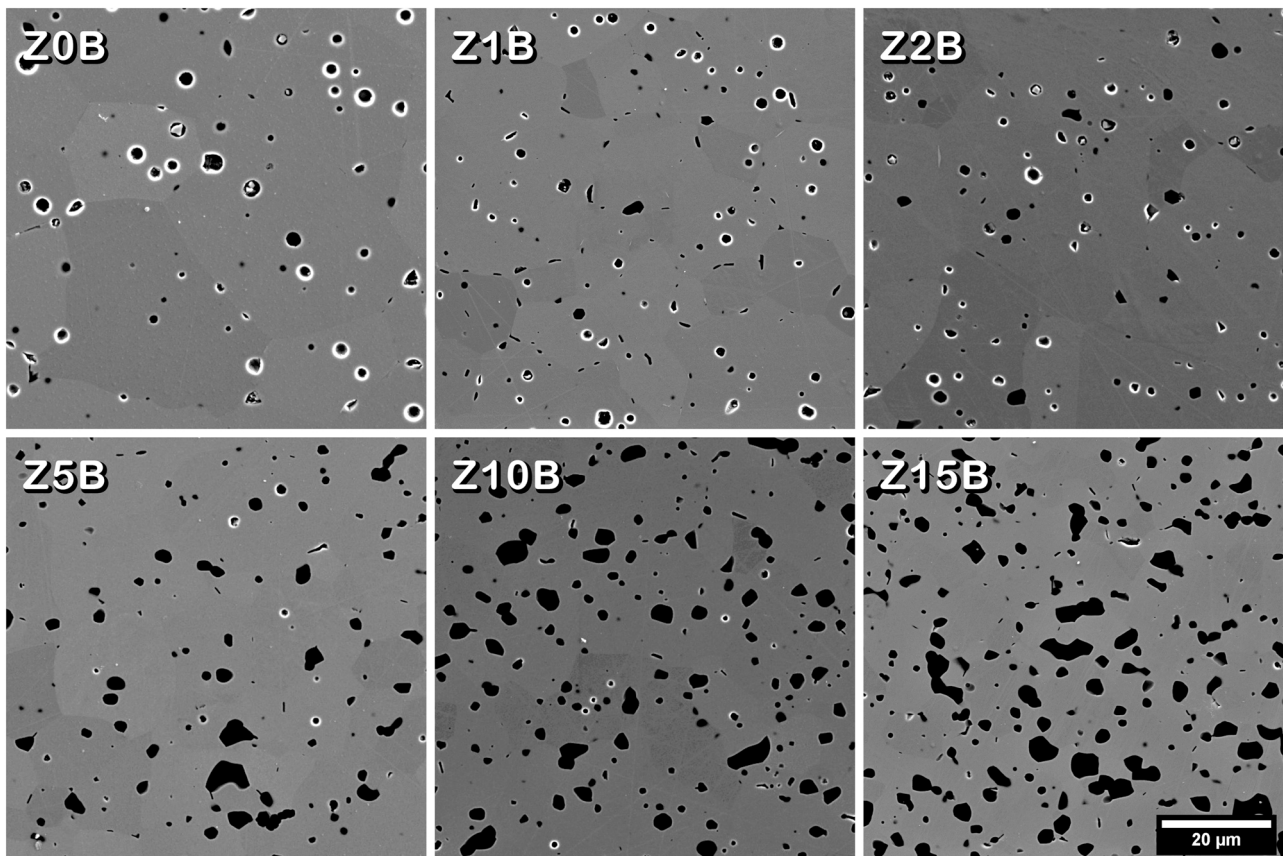
Fig. 1. Secondary electron micrographs of the polished cross-sections for the ZrB$_2$-B$_4$C ceramics hot-pressed at 2100 °C at 32 MPa in flowing Ar atmosphere.
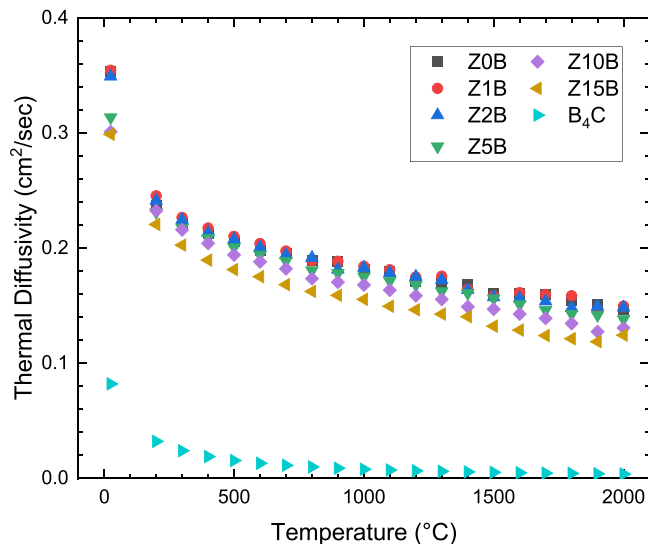

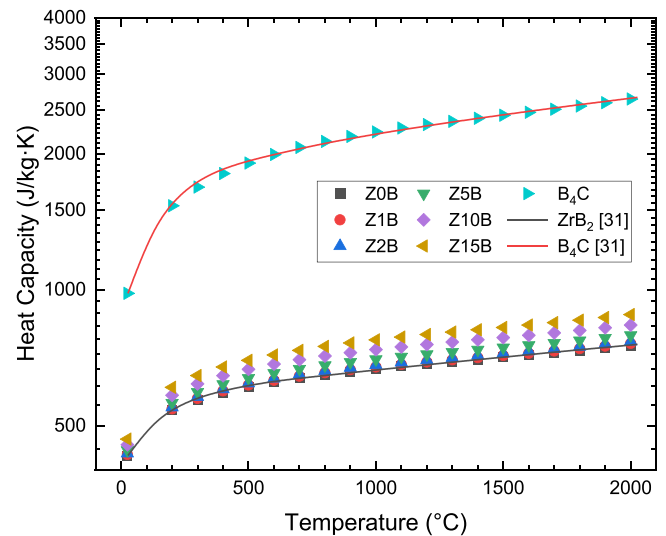**Fig. 2.** Thermal diffusivity of the hot-pressed ZrB$_2$-B$_4$C ceramics as a function of temperature.

Fig. 3. Heat capacity as a function of temperature for ZrB$_2$-TiB$_2$ ceramics along with handbook values for pure ZrB$_2$ and TiB$_2$ [31].

which was 97.2% of the theoretical density. Additions of as little as 1 vol % B$_4$C increased the relative density of the resulting ceramics. For example, the bulk density of Z1B was 6.02 g/cm^3, which was > 99% relative density. For all of the ZrB$_2$-B$_4$C specimens, relative density values were > 99% of the theoretical densities based on the nominal compositions. Additions of B$_4$C decreased the theoretical density of the ZrB$_2$-B$_4$C ceramics from 6.10 g/cm^3 for nominally pure ZrB$_2$ to as low as 5.62 g/cm^3 for Z15B.

ZrB$_2$ grain size, the distribution of B$_4$C, and the amount and location of porosity were investigated using SEM (Fig. 1). The average grain size for nominally pure ZrB$_2$, Zr0B, was 22.4 μm. The addition 1 vol% of B$_4$C reduced the average grain size to 14.5 μm. The reduction in grain size was attributed to a combination of removing surface oxides, reducing grain coarsening at elevated temperatures, and grain pinning by the B$_4$C particles. Larger additions of B$_4$C were more effective at reducing the average ZrB$_2$ grain size. For example, Z5B had an average grain size of 12.0 μm. As B$_4$C content increased, the average grain size continued to
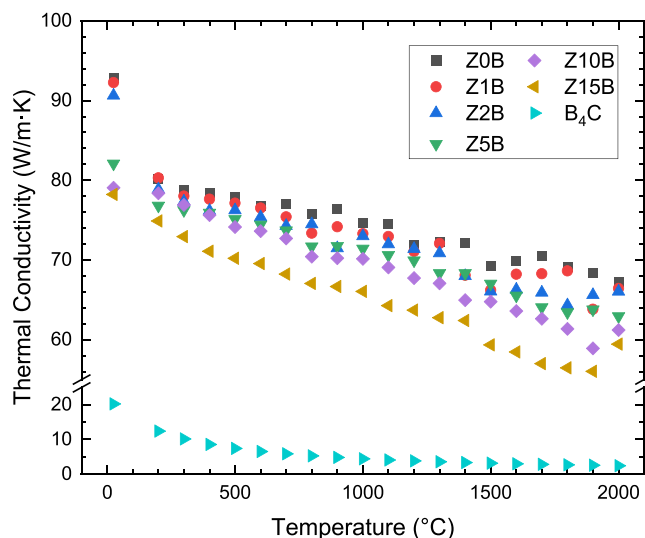
Fig. 4. Thermal conductivity of the hot-pressed ZrB2-B4C ceramics as a function of temperature calculated from the measured thermal diffusivity and calculated heat capacity and bulk density.

decrease to a minimum of 5.4 μm for Z15B. The decrease in average grain size with increasing B$_4$C content was attributed to the increase in pinning of ZrB$_2$ grain growth with the increasing volume fraction of second phase particles [30]. Regardless of the amount of B$_4$C, SEM analysis revealed that the average size of B$_4$C inclusions in the ZrB$_2$ matrix was 3.8 ± 1 μm. SEM analysis also showed that B$_4$C was present as well dispersed, isolated particles in the ZrB$_2$ matrix. The addition of B$_4$C improved the relative density of the ZrB$_2$ ceramics and reduced the average grain size of the final ceramics through a combination of reaction with/removal of surface oxides and grain pinning.

Thermal conductivity was determined from measured thermal diffusivity values combined with calculated heat capacity and density values. Fig. 2 shows the thermal diffusivity as a function of temperature for the ZrB$_2$-B$_4$C ceramics. The values of heat capacity (Fig. 3) for each composition were consistent with values predicted using a volumetric rule of mixtures calculation with the accepted values for each phase in the NIST-JANAF tables [31]. Fig. 4 shows the thermal conductivity as a function of temperature for the ZrB$_2$-B$_4$C ceramics. For nominally pure ZrB$_2$, the thermal conductivity decreased from 93 W/m·K at 25 °C to 81 W/m·K at 200 °C. Above 200 °C, the thermal conductivity decreased linearly from 80 W/m·K at 200 °C to 67 W/m·K at 2000 °C with a slope of -6.9×10^{-3} W/m·K^2. Additions of 1 or 2 vol% of B$_4$C did not change the room temperature thermal conductivity significantly as the value was 93 W/m·K for both Z1B and Z2B. The thermal conductivities of these compositions, along with Z0B, decreased to 67 W/m·K at 2000 °C. Since B$_4$C has a lower thermal conductivity than ZrB$_2$, its addition should lower the thermal conductivity of the composite ceramics. The lack of change in thermal conductivity of Z1B and Z2B compared to Z0B could be attributed to the increased relative density and decreased oxide impurity contents of Z1B and Z2B compared to Z0B. Although oxygen content of the hot-pressed ceramics was not measured, removal of surface oxide impurities in transition metal diborides during sintering by boro-carbothermal reduction with B$_4$C is a well-understood phenomenon [30].

The addition of more than 2 vol% B$_4$C decreased the thermal conductivity of the resulting ceramics. For instance, Z5B had a thermal conductivity of 83 W/m·K at 25 °C that decreased to 64 W/m·K at 2000 °C. Adding more B$_4$C, as in the cases of Z10B and Z15B, further decreased the thermal conductivity at 25 °C to 81 W/m·K and 79 W/m·K, respectively. Excess B$_4$C was present as a second phase in the ZrB$_2$ matrix for compositions batched with 2 vol% B$_4$C or more. As all of the B$_4$C-containing ceramics had relative densities > 99%, the decreasing
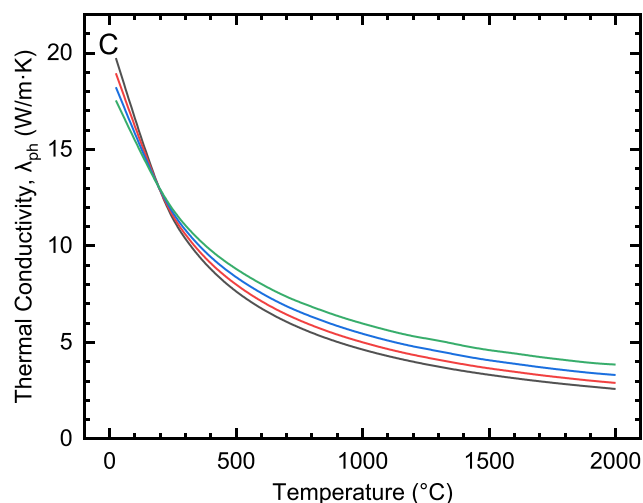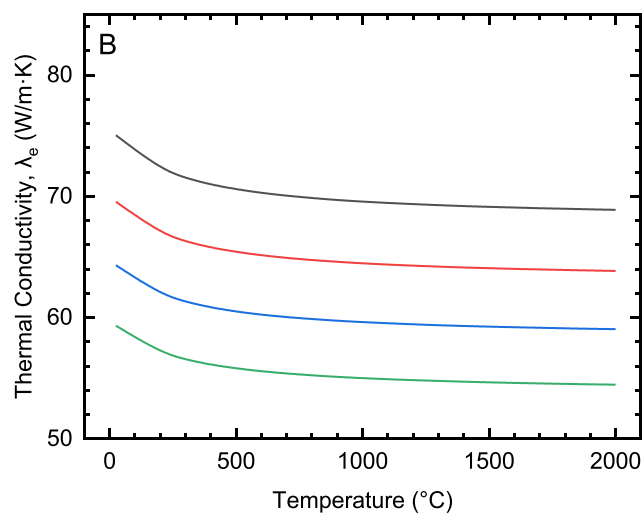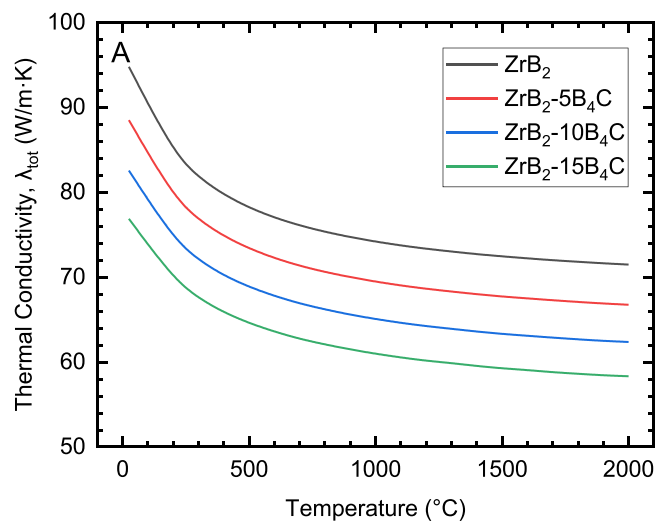

Fig. 5. The calculated model total thermal conductivity (A), and the electron (B) and phonon (C) contributions to thermal conductivity for the ZrB$_2$ – 0, 5, 10, and 15 vol% B$_4$C isopleths.

thermal conductivity with increasing B$_4$C content was a result of B$_4$C having a lower thermal conductivity compared to ZrB$_2$.

The calculated total thermal conductivity along with the electron and phonon contributions to thermal conductivity predicted by the model are shown in Fig. 5. The model follows the expected trend of
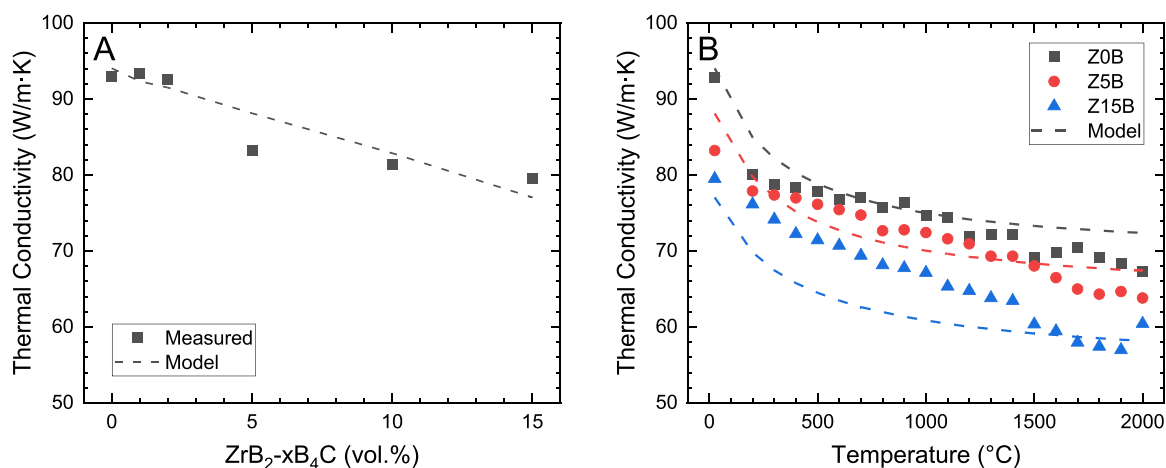
Fig. 6. Comparison of model predictions (lines) to measured values (points) of thermal conductivity at (A) room temperature and (B) as a function of temperature for ZrB2-B4C ceramics.
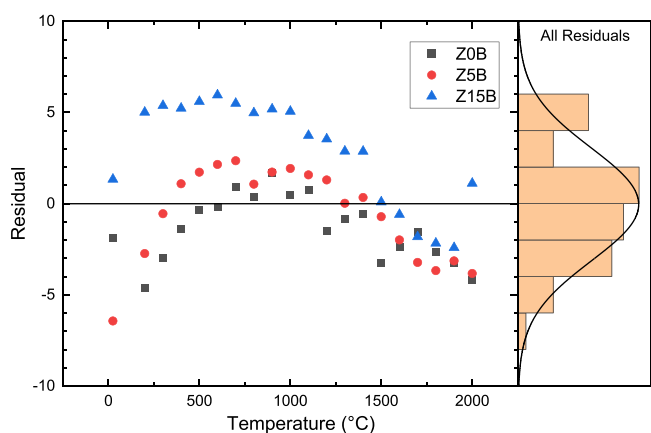

Fig. 7. Residuals of the fitted model as a function of temperature and B_4C content.

decreasing thermal conductivity with increasing temperature. In addition, the model predicts decreasing thermal conductivity with increasing B_4C content as a result of a suppression in the electron contribution to thermal conductivity due to the lower conductivity of B_4C. The decrease in total thermal conductivity with increasing B_4C addition is slightly slowed by an increase in the phonon contribution with increasing B_4C content. Model predictions were compared to measured thermal conductivity values. In Fig. 6, the 25 °C thermal conductivity values predicted by the model were compared to experimental values. For Z0B, the model predicted a thermal conductivity of 94 W/m·K compared to the experimental value of 93 W/m·K. Likewise, the model predicted that the 25 °C thermal conductivity would decrease to 77 W/m·K for Z15B due to the presence of B_4C and the decrease in grain size, which was close to the experimental value of 80 W/m·K. The factors that most impacted the room temperature conductivity were the B_4C addition on the electron contribution and the ZrB_2 grain size on the phonon contribution.

Thermal conductivity was predicted as a function of temperature. The model predicted that the thermal conductivity of Z0B was 72 W/m·K at 2000 °C, compared to the experimental value, 67 W/m·K (Fig. 6). The model predicted thermal conductivity values for ZrB_2-B_4C ceramics well ($R^2 = 0.998$) with the exception of ZrB_2 with > 5 vol% B_4C. Observing the residual plot (Fig. 7) shows a parabolic bias with temperature, centered around 1000 °C, and a negative bias with increasing B_4C content. For these compositions, the model deviated from experimental values between 200 °C and 800 °C, with a maximum difference of 7 W/m·K. A potential reason for this discrepancy may be due to more

interaction of B_4C than anticipated based on the current model. This model as a whole revealed that while the electron contribution to thermal conductivity was solely due to ZrB_2, the phonon contribution was higher than expected based solely on the volume fraction of B_4C in the composite.

4. Conclusions

The thermal conductivity values of ZrB_2-B_4C ceramics were modeled and compared to experimental data to determine how isolated second phases affected high temperature behavior. The addition of B_4C to ZrB_2 decreased the grain size from 22 μm for pure ZrB_2 to 5.4 μm for Z15B. The addition of B_4C also decreased the thermal conductivity of the ZrB_2 ceramics to 79.6 W/m·K for Z15B at 25 °C compared to 93.0 W/m·K for Z0B. In each case, the thermal conductivity decreased quickly from 25 °C to 200 °C. Above 200 °C, the thermal conductivity decreased linearly to 2000 °C. At 2000 °C, the thermal conductivity of Z0B was 67.3 W/m·K and decreased to 60.5 W/m·K for Z15B.

A model for the thermal conductivity was developed using B_4C content, ZrB_2 grain size, and temperature and was in agreement with measured values. The developed model revealed that B_4C improved the phonon contribution to thermal conductivity and decreased the electron contribution, which decreased the total thermal conductivity compared to pure ZrB_2. A discrepancy in the model was observed for B_4C content greater than 5 vol%, perhaps from greater interaction of the B_4C than anticipated. The model can calculate the expected thermal conductivity for ZrB_2 with a non-electrically conducting second phase based on the volume fraction of second phase, and the conductivities of ZrB_2 and the second phase as a function of temperature.

Declaration of Competing Interest

The authors declare that they have no known competing financial interests or personal relationships that could have appeared to influence the work reported in this paper.

References

[1] R.A. Cutler, Engineering properties of borides, in: S.J.S. Schneider Jr. (Ed.), Ceramics and Glasses: Engineered Materials Handbook, ASM International, Materials Park, OH, 1991, pp. 787–803.

[2] R. Telle, L.S. Sigl, K. Takagi, Boride-based hard materials, in: R. Riedel (Ed.), Handbook of Ceramic Hard Materials, Wiley-VCH, Weinheim, Germany, 2000, pp. 802–945.

[3] X. Zhang, X. Luo, J. Han, J. Li, W. Han, Electronic structure, elasticity and hardness of diborides of zirconium and hafnium: first principles calculations, Comput. Mater. Sci. 44 (2) (2008) 411–421.

[4] S. Guo, Y. Kagawa, T. Nishimura, H. Tanaka, Thermal and electric properties in hot-pressed ZrB_2–$MoSi_2$–SiC composites, J. Am. Ceram. Soc. 90 (7) (2007) 2255–2258.

[5] L. Zhang, D.A. Pejaković, J. Marschall, M. Gasch, Thermal and electrical transport properties of spark plasma-sintered HfB_2 and ZrB_2 ceramics, J. Am. Ceram. Soc. 94 (8) (2011) 2562–2570.

[6] M.M. Opeka, I.G. Talmy, J.A. Zaykoski, Oxidation-based materials selection for $2000°C$ + hypersonice aerosurfaces: theoretical considerations and historical experience, J. Mater. Sci. 39 (19) (2004) 5887–5904.

[7] R.P. Tye, E.V. Clougherty, The thermal and electrical conductivities of some electrically conducting compounds, in: C.F. Bonilla (Ed.), Proceedings of the Fifth Symposium on Thermophysical Properties, American Society of Mechanical Engineers, Newton, MA, 1970, pp. 396–401.

[8] W.G. Fahrenholtz, G.E. Hilmas, I.G. Talmy, J.A. Zaykoski, Refractory diborides of zirconium and hafnium, J. Am. Ceram. Soc. 95 (5) (2007) 1347–1364.

[9] A. Rezaie, W.G. Fahrenholtz, G.E. Hilmas, Effect of hot pressing time and temperature on the microstructure and mechanical properties of ZrB_2-SiC, J. Mater. Sci. 42 (8) (2007) 2735–2744.

[10] A.L. Chamberlain, W.G. Fahrenholtz, G.E. Hilmas, High-strength zirconium diboride-based ceramics, J. Am. Ceram. Soc. 87 (6) (2004) 1170–1172.

[11] D. Kalish, E.V. Clougherty, Densification mechanisms in high-pressure hot-pressing of HfB_2, J. Am. Ceram. Soc. 52 (1) (1969) 26–30.

[12] S. Zhu, W.G. Fahrenholtz, G.E. Hilmas, S.C. Zhang, Pressureless sintering of carbon-coated zirconium diboride powders, Mater. Sci. Eng., A 459 (1–2) (2007) 167–171.

[13] W.G. Fahrenholtz, G.E. Hilmas, S.C. Zhang, S. Zhu, Pressureless sintering of zirconium diboride: particle size and additive effects, J. Am. Ceram. Soc. 91 (5) (2008) 1398–1404.

[14] J.W. Zimmermann, G.E. Hilmas, W.G. Fahrenholtz, R.B. Dinwiddie, W.D. Porter, H. Wang, Thermophysical properties of ZrB_2 and ZrB_2–SiC ceramics, J. Am. Ceram. Soc. 91 (5) (2008) 1405–1411.

[15] W.-B. Tian, Y.-M. Kan, G.-J. Zhang, P.-L. Wang, Effect of carbon nanotubes on the properties of ZrB_2–SiC ceramics, Mater. Sci. Eng. A 487 (1) (2008) 568–573.

[16] J.M. Lonergan, W.G. Fahrenholtz, G.E. Hilmas, Zirconium diboride with high thermal conductivity, J. Am. Ceram. Soc. 97 (6) (2014) 1689–1691.

[17] S. Guo, T. Nishimura, Y. Kagawa, Preparation of zirconium diboride ceramics by reactive spark plasma sintering of zirconium hydride-boron powders, Scr. Mater. 65 (2011) 1018–1021.

[18] M. Gasch, S. Johnson, J. Marschall, Thermal conductivity characterization of hafnium diboride-based ultra-high-temperature ceramics, J. Am. Ceram. Soc. 91 (5) (2008) 1423–1432.

[19] A. Eucken, Thermal conductivity of ceramic refractory materials; calculation from thermal conductivity of constituents, Ceram. Abstr. (1932) 353–360.

[20] L.M. Clark, R.E. Taylor, Radiation loss in the flash method for thermal diffusivity, J. Appl. Phys. 46 (2) (1975) 714–719.

[21] K. Shinzato, T. Baba, A laser flash apparatus for thermal diffusivity and specific heat capacity measurements, J. Therm. Anal. Calor. 64 (1) (2001) 413–422.

[22] Y.S. Touloukian, R.K. Kirby, R.E. Taylor, T.Y.R. Lee, Thermal Expansion - Nonmetallic Solids, IFI/Plenum Data Company, New York, NY, 1977.

[23] M. Bouchacourt, F. Thevenot, The correlation between the thermoelectric properties and stoichiometry in the boron carbide phase B_4C-$B_10.5C$, J. Mater. Sci. 20 (4) (1985) 1237–1247.

[24] E.W. Neuman, G.J.K. Harrington, G.E. Hilmas, W.G. Fahrenholtz, Elevated temperature electrical resistivity measurements of zirconium diboride using the van der Pauw method, J. Am. Ceram. Soc. 102 (12) (2019) 7397–7404.

[25] C.-N. Sun, M.C. Gupta, W.D. Porter, Thermophysical properties of laser-sintered Zr–ZrB_2 cermets, J. Am. Ceram. Soc. 94 (8) (2011) 2592–2599.

[26] R. Franz, G. Wiedemann, Ueber die Wärme-Leitungsfähigkeit der Metalle, Ann. Phys. 165 (8) (1853) 497–531.

[27] E.W. Neuman, M. Thompson, W.G. Fahrenholtz, G.E. Hilmas, Thermal properties of ZrB_2-TiB_2 solid solutions, J. Eur. Ceram. Soc. 41 (15) (2021) 7434–7441.

[28] A. Eucken, Allgemeine Gesetzmäßigkeiten für das Wärmeleitvermögen verschiedener Stoffarten und Aggregatzustände, Forschung auf dem Gebiet des Ingenieurwesens A 11(1), 1940, pp. 6–20.

[29] D.S. Smith, S. Fayette, S. Grandjean, C. Martin, R. Telle, T. Tonnessen, Thermal resistance of grain boundaries in alumina ceramics and refractories, J. Am. Ceram. Soc. 86 (1) (2003) 105–111.

[30] D. Sciti, L. Silvestroni, V. Medri, F. Monteverde, Sintering and densification mechanisms of ultra-high temperature ceramics, in: W.G. Fahrenholtz, E. J. Wuchina, W.E. Lee, Y. Zhou (Eds.), Ultra-High Temperature Ceramics: Materials for Extreme Environment Applications, John Wiley & Sons, Inc, Hoboken, NJ, 2014, pp. 112–143.

[31] M.W. Chase, NIST-JANAF Thermochemical Tables, fourth ed., American Institute of Physics, Woodbury, NY, 1998.